

README for the Geant4 Lunar Albedo Computed Environment (GLACE) Model

Mark D. Looper, The Aerospace Corporation

Version 1.0, May 2, 2023

1. Lunar Albedo Simulation Geometry and Parameters

The purpose of the GLACE model is to encapsulate the results of hundreds of processor-years of Geant4 simulations (Agostinelli et al., 2016) of lunar albedo – energetic secondary particles that result from the impact on the lunar surface of primary ions arriving from space – into a form that will enable other researchers to perform calculations of particle flux, radiation dose, etc., without having to redo all those simulations. The model consists of results for sixteen target geometries, one representing dry ferroan anorthosite (FAN) and the rest representing a surface layer of hydrogen-bearing FAN above a dry FAN substrate, with three surface compositions (1% by weight of hydrogen, 10% of hydrogen, or 9% of water which combines 1% hydrogen with 8% oxygen) and five depths of the hydrogen-bearing surface layer (1 mm, 1 cm, 10 cm, 1 m, 10 m).

A density of 3.0 g/cc was assigned to all materials in the simulations; expressing these depths as column mass densities, i.e., distances multiplied by volume density (0.3, 3, 30, 300, and 3000 g/cm²), allows them to be converted into equivalent depths in materials with other densities, e.g., loose regolith with many voids and lower average density. Preliminary simulations with other kinds of dry rock-like targets have shown that the results vary only slightly with composition, so the selection of FAN as the baseline material does not result in much loss of generality. In particular, for studies comparing the effects of varying amounts of surface hydrogenation on the lunar albedo, any slight differences between results for different possible choices of base material should cancel out in such a comparison.

For each geometry, the upper surface of the slab of regolith was bombarded with an isotropic flux of energetic primary ions, with a set of simulations performed for the most common isotope of each element from $Z = 1$ to 28 (hydrogen to nickel), and also for ³He. 200 energies were simulated for each ion species, logarithmically spaced from 10 MeV/nuc to 10 GeV/nuc (to 100 GeV/nuc for protons). A set of simulation runs using each of 20 different random-number-generator seeds, to enable estimation of statistical errors, was executed for each species and energy. The number of incident particles simulated per run (a given incident species and energy, and a given random-number-generator seed, for a given target geometry) varied from 10⁷ for protons to 10⁴ for the least abundant ion species at the lowest energies, and declined in inverse proportion to incident-ion energy.

Geant4 allows tracking of any energetic particle through an arbitrary 3D geometry, with the user having access to all properties of the particle at any point along its track. The physics models governing the particle transport through the geometry in Geant4 can be as complete as computer power allows; however, these models are continually being refined by the Geant4

developers, and we found that even using a different patch level for the same release of the code could result in differences in the results that were comparable to some of the very small differences between albedo from different patterns of surface hydrogenation that we were trying to study. Thus, for definiteness, all simulations for GLACE were performed using version 10.7 of Geant4, patch level 1 (geant4.10.07.p01). Hadronic physics, including nuclear interactions of heavy projectile ions on heavy targets, was modeled using the “Shielding” reference physics list, and the slowest-running but most accurate electromagnetic physics model “EMZ” was also used: “Shielding_EMZ” is the name of the combined reference physics list that can be invoked by others who wish to produce additional results that will be directly comparable with those in GLACE, again with the stipulation that geant4.10.07.p01 should also be used.

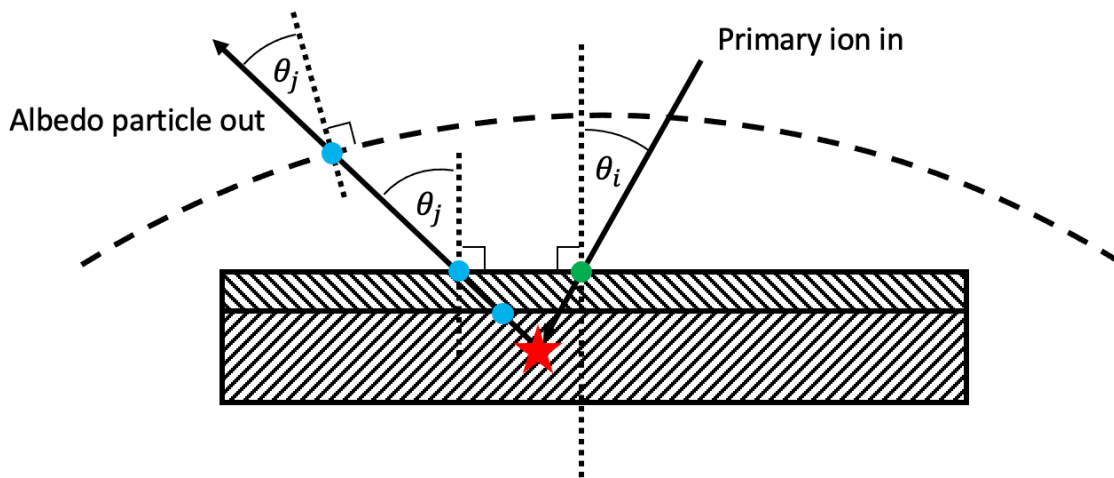


Figure 1: Schematic drawing of simulation geometry, not to scale. The actual target slab had a combined thickness (both layers) of 20 m and was 4 km wide in each horizontal direction, while the spherical counting surface in space passing 20 km above the green input point had a radius 20 km larger than the lunar radius, or 1758 km total. See main text for further description.

Figure 1 schematically shows the simulation geometry, not to scale. The incident particles were launched into a point (green dot) at the center of the upper surface of a rectangular slab of FAN, or of a layer of hydrogenated FAN above a dry layer (the two crosshatched boxes), with a combined thickness of 20 m and horizontal dimensions of 4 km x 4 km. This was sufficient to contain the nuclear and electromagnetic showers being simulated. This slab of material was embedded in a volume of vacuum sufficiently large to enclose a surface in empty space corresponding to the portion of a sphere around the Moon, with a radius 20 km larger than the 1738 km radius of the Moon (dashed line), that would appear above the horizon from the position of the bombarded slab. Escaping particles were tabulated at the surface of the slab (blue dot on slab), and also when particles crossed this spherical section representing 20 km above the lunar surface (upper blue dot) to account for the decay of unstable particles (in particular, all pions and almost all muons) on their way to an orbiting spacecraft.

Note that the secondary particle's off-normal angle θ_j is larger at the surface than it is for the same trajectory where it crosses the tabulation sphere at 20 km altitude. This is related to the fact that, for example, the Moon only extends out to 81.3° from the nadir as seen from 20 km altitude, vs. 90° as seen from the surface, so that all angles are compressed as seen from above the surface. If the angular distribution at a different altitude is desired, the angles in the model files can be scaled by simple trigonometry, with the values of the flux (or rather, the model flux kernels from which flux will be calculated) unchanged according to Liouville's theorem. However, it is important to do this scaling starting with the model results tabulated at 20 km altitude rather than at the surface, in order to account for decay of unstable particles (mostly adding to electrons and positrons) on the way up.

Escaping particles at these two altitudes, 0 and 20 km, were sorted into 16 groups: γ , e^- , e^+ , μ^- , μ^+ , π^- , π^+ , neutrons, ^1H , ^2H , ^3H , ^3He , ^4He , heavier isotopes of helium, ions heavier than helium, and all other miscellaneous subatomic particles (kaons, sigmas, etc.) except neutrinos. In addition, upward-going neutrons were tabulated at a third "altitude," the interface between the upper (hydrogenated FAN) and lower (dry FAN) layers, or 10 cm below the surface for the entirely dry case (lowest blue dot in Figure 1), to study conversion of their energy into that of albedo protons in the upper layer. Finally, for neutrons and protons escaping from the surface, the depth of origin (red star) and the creation process for each particle were tabulated, to study the depths beneath the lunar surface that are probed by observations of each of these kinds of particle at different energies and angles.

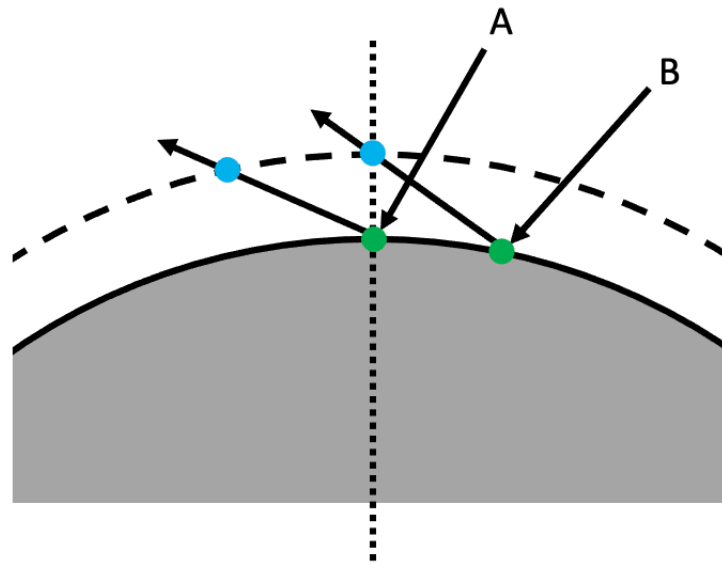


Figure 2: Schematic drawing of symmetry of the geometry of which a segment is represented by the simulation, not to scale. Simulated primary particles were incident on a common point (green dot), with albedo particles reaching the 20-km-altitude tabulation surface some distance away horizontally (blue dot), as represented by inbound and outbound trajectories labeled "A". The existence of an equivalent trajectory pair like that labeled "B" allows us to map flux at all angles over the spherical tabulation surface (dashed line) to a common point, as discussed in the main text.

For the escaping particles tabulated at and below the surface of the target slab, intermediate results from the simulation show that their points of escape (blue dots in Figure 1) are horizontally separated from the point of incidence of the primary particle (green dot) by a

distance that is small compared with the radius of the Moon. Thus we can consider all energy and angular distributions of these particles to represent the distributions that would be measured at a single point on the lunar surface. However, this horizontal separation can be tens or hundreds of km for the point where an albedo particle crosses the spherical surface at 20 km altitude, as shown schematically in Figure 2, with the inbound/outbound trajectory pair labeled “A”. For a spherical Moon and isotropic incident flux, though, an equal number of particles will have trajectories rotated and displaced around the curve of the Moon to cross the tabulation surface at the same point as particles coming straight up from the simulated incident point, as shown by the pair of trajectories labeled “B”. Thus we can likewise consider the energy and angular distributions of the particles tabulated on the 20-km-altitude spherical surface in the simulation to represent the distributions at a single point 20 km directly above the incidence point in the simulation (blue dot falling on the dotted line in Figure 2), as long as we calculate the angle θ_j of the tabulated albedo particles relative to the local radius vector at 20 km altitude, as shown in Figure 1, rather than relative to the vertical radius vector through the point of primary-particle incidence.

2. Quantities Tabulated in the Model

The model collects and normalizes the simulation results into kernels, which can be convolved with any desired incident ion spectra (say, those from a particular solar energetic particle event, or the galactic cosmic ray flux during specific conditions of solar modulation) to evaluate the lunar albedo fluxes that result. In the discussion to follow, we will consider only a single target geometry, a single tabulation altitude (surface, 20 km altitude, or subsurface), and a single incident ion species; a user can sum over the results for all ion species to study the aggregate effect of a complete incident solar-particle or cosmic-ray population on the albedo particles from the set of observation conditions (lunar target geometry, altitude) of interest.

2.1 Energy/Angle Distributions of Multiple Albedo Species

The main observable quantities that can be calculated using GLACE are the upward-going energy-angle distributions for the sixteen groups of secondary particles listed in Section 1 at the surface, at 20 km altitude, and (for the neutrons only) below the surface. Again considering just a single incident ion species labeled i , and a single target geometry and tabulation altitude, let $j_i(E_i)$ be the directional flux in particles per ($\text{cm}^2 \text{ sr sec MeV/nuc}$) of ion species i arriving from space at energy E_i in MeV/nuc. Since the flux is taken to be isotropic in these simulations, $j_i(E_i)$ is not a function of position or direction. Let $q_j(E_i, E_j, \theta_j)$ be the directional fluence of a particular secondary-particle species j that arises from a given isotropic fluence per unit area of species i at energy E_i , divided by that incident fluence. Its units will be particles of species j per (sr MeV/nuc) or per (sr MeV) depending on whether that species is an ion or not (the “per cm^2 ” in numerator and denominator cancel out). In addition to the energy E_i of the incident particles, it is a function of secondary-particle energy E_j and of the angle θ_j from the vertical direction to each secondary particle’s direction of travel as in Figure 1, but by

symmetry about the vertical axis it will not be a function of the azimuthal angle φ_j about that axis.

Consider the isotropic primary particles to be incident on a small surface area element dA over a time interval dt , and within a small energy interval dE_i around E_i . Then

$$N_i(E_i) = j_i(E_i)dE_idGdt = \pi j_i(E_i)dE_idAdt \quad (1)$$

is the number of particles striking the surface, where the factor of π (steradians) comes from the integral over all incident-particle arrival directions of the solid angle within a small angle range $d\theta_i$ around each incident-particle zenith angle θ_i , times the projection of the surface area element normal to that zenith angle:

$$dG = \int_0^{\pi/2} d\theta_i 2\pi \sin \theta_i \cos \theta_i dA = \pi dA \quad (2)$$

Then the fluence of secondary particles from this quantity of primary particles will be given by

$$Q_j(E_i, E_j, \theta_j) = q_j(E_i, E_j, \theta_j) \frac{N_i(E_i)}{dA} = \pi q_j(E_i, E_j, \theta_j) j_i(E_i) dE_i dt \quad (3)$$

in units of secondary particles per (cm² sr MeV) or (cm² sr MeV/nuc). If we integrate over dE_i and divide out the observation time dt , we will obtain the directional flux of secondary particles that results from an incident flux $j_i(E_i)$ of primary particles:

$$J_j(E_j, \theta_j) = \frac{1}{dt} \int_0^\infty dE_i \pi q_j(E_i, E_j, \theta_j) j_i(E_i) dt = \int_0^\infty dE_i R_j(E_i, E_j, \theta_j) j_i(E_i) \quad (4)$$

$R_j(E_i, E_j, \theta_j)$, which will be equal to π sr multiplied by $q_j(E_i, E_j, \theta_j)$ and which will be in units of secondary particles per MeV/nuc or per MeV, is the response kernel that is tabulated for secondary-particle energy-angle distributions in the GLACE dataset. Users can convolve it with an incident flux of ions $j_i(E_i)$ as in equation (4) and, summing over all incident species i , can build up the total energy-angle directional flux distribution of secondary-particle species j .

The response function is stored as a multi-dimensional matrix. There 200 logarithmically-spaced bins in E_i from 10 MeV/nuc to 10 GeV/nuc for all incident ion species except protons, and from 10 MeV/nuc to 100 GeV/nuc for protons. 600 bins in E_j are also logarithmically spaced, from 0.1 MeV to 100 GeV for most secondary particles; for secondary ions heavier than protons the energy limits are 0.1 MeV/nuc and 100 GeV/nuc, and for neutrons GLACE tabulates down to thermal energies, 10⁻⁴ eV to 100 GeV. Finally, there are 90 linearly-spaced bins in θ_j from 0° to 90° relative to the surface normal.

2.2 Energy/Angle/Source-Depth Distributions of Protons and Neutrons

The above discussion only considered secondary particles at the points of observation, whether on the surface, above it, or (for neutrons) below it. For protons and neutrons, the simulations also logged the depth at which the track of each escaping proton or neutron originated, and the physical process that created that track. Adding another dimension to the response function defined above, say $S_j(E_i, E_j, D_j, \theta_j)$ where D_j is the depth of origin of the escaping particle's track below the lunar surface, would multiply the data volume of the GLACE model file many times over, though this could be reversed by tabulating instead the response integrated over another of the variables, say θ_j . In order to keep at least coarse angular resolution, so that users can examine how deeply into the surface observations of neutrons or protons at different energies and angles can probe, GLACE instead sums response vs. the angle θ_j into coarse bins of 0°-30°, 30°-60°, and 60°-90°. Thus we differentiate the response with depth, so that

$$R_j(E_i, E_j, \theta_j) = \int_0^{\infty} dD_j S_j(E_i, E_j, D_j, \theta_j) \quad (5)$$

defines an energy/angle/depth kernel $S_j(E_i, E_j, D_j, \theta_j)$, and

$$Q_j(E_j, D_j, \theta_j) = \int_0^{\infty} dE_i S_j(E_i, E_j, D_j, \theta_j) \quad (6)$$

gives the observable secondary-particle flux differentiated by depth of origin, $Q_j(E_j, \theta_j, D_j)$. As mentioned in Section 1, the simulated target material has a volume mass density of 3.0 g/cc, and scaling the measurement of depth from length units to column mass density units by multiplying it by the volume mass density allows it to be related to depths in materials of other densities. Thus we take the dimensions of D_j to be g/cm² and those of $S_j(E_i, E_j, \theta_j, D_j)$ to be secondary particles per [MeV g/cm²], or per [MeV/nuc g/cm²] for secondary ions heavier than protons.

Again, GLACE stores this response function as a multi-dimensional matrix. The binning in E_i and E_j is the same for $S_j(E_i, E_j, D_j, \theta_j)$ as for $R_j(E_i, E_j, \theta_j)$ in Section 2.1, and as mentioned above θ_j is divided here into 3 linearly-spaced bins. D_j is tabulated in 250 logarithmically-spaced bins from 3×10^{-2} to 3×10^3 g/cm² below the surface (100 microns to 10 meters in the simulation geometry), except that the first bin goes all the way up to the surface (zero depth). The energy/angle response results were tabulated at the lunar surface and 20 km above it and, for neutrons, beneath the surface; energy/angle/source-depth response results are provided only for protons and neutrons escaping the surface, but they are subdivided instead by creation process. The many physical processes whose generation of secondary particles is modeled by Geant4 can be sorted into inelastic processes and elastic processes. Protons and neutrons alike can result from inelastic processes, but in these simulations only protons escaped to space after being launched by elastic processes, usually the impact of a neutron coming from below and transferring its energy to a hydrogen nucleus in the upper layer. In addition, for proton (¹H)

incident ions only, GLACE tabulates protons that scatter enough after striking the surface that they turn around and escape to space so as to be counted among the albedo particles. Because origin depth is zero for all such particles, their full energy/angle response $R_j(E_i, E_j, \theta_j)$ is tabulated, representing a subset of the response in the main dataset for proton albedo produced by incident protons.

3. Structure of the Stored Model Output

3.1 File Names and Organization

The GLACE model is stored as a large set of JSON-formatted ASCII files, which can readily be imported by many data-analysis software packages. These model files are accompanied by some sample results showing realistic particle fluxes produced using the model, stored as both JSON files and PNG plots, which users can compare with the results of their own calculations to check their importing and use of the model components. All these files are collected into 96 zipfiles, six for each of the sixteen target geometries, as detailed in Section 1. The individual zipfiles range in size from 379 MB to 6 GB; the total volume of data is 206 GB compressed, 2.6 TB uncompressed. Altogether, the GLACE model comprises 16,720 kernel files, along with 3,744 sample result files.

The JSON format is easy for machines or humans to read, and compresses well; however, sparse matrices have long sequences of "...0.0,0.0,0.0,..." in uncompressed form, which creates large files. We decided that the advantages of JSON outweighed this inefficiency, but we broke the model into 96 zipfiles so that users need not waste space storing, or bandwidth downloading, parts of the model in which they are not interested. The compressed and uncompressed lengths of each of the 96 zipfiles are listed in the Appendix, so that users can allocate resources to download and unzip the subsets of the model that they wish to use. For example, users interested only in the baseline case of a dry FAN target can download only the six zipfiles corresponding to that target geometry, and if interest is further restricted to a subset of albedo particle species then only one or a few of those six zipfiles would be needed.

3.1.1 Energy/Angle Kernels

The model's files for the main energy/angle kernels, containing the responses $R_j(E_i, E_j, \theta_j)$ as defined in equation (4), will have names and filepaths like

dry_10cm_electrons/electrons_20_km_altitude/ion_28_58.json

The contents of the files will be discussed in section 3.2, but the directory and file names encode information as well. The base directory for the example above, "dry_10cm_electrons", is the folder that was zipped into "dry_10cm_electrons.zip," and all such base directories have similarly-structured names. The three pieces of the name, separated by underscores, tell what target geometry and particles are addressed by the contents of that directory and zipfile. First

is the composition of the upper layer, one of “dry,” “h1pct,” “h10pct,” and “h2o9pct” to identify the four possibilities described at the start of Section 1. Second is the thickness of the upper layer, one of “1mm,” “1cm,” “10cm,” “1m,” and “10m,” except that “dry” is only paired with “10cm” as in the example above. Third is the albedo species covered, one of “electrons,” “gammas,” “neutrons,” “protons,” or “other,” with the last encompassing the rest of the particle categories listed in Section 1 (e^+ , μ^- , μ^+ , π^- , π^+ , ^2H , ^3H , ^3He , ^4He , heavier isotopes of helium, ions heavier than helium, and miscellaneous).

Within each of these base directories are subdirectories containing the model files for each of the tabulation altitudes shown as blue dots in Figure 1. The subdirectory names will tell which individual particle category and which altitude is addressed. The first part of the name will be “electrons,” “gammas,” “neutrons,” or “protons” for all files in those respective base directories, and one of “positrons,” “mu_minus,” “mu_plus,” “pi_minus,” “pi_plus,” “deuterons,” “tritons,” “helium_3,” “alphas,” “heavy_helium,” “z_gt_2,” or “misc” for files in the base directories ending with “_other.” The second part of the name identifies the tabulation altitude: “surface” or “20_km_altitude,” and for neutrons only, “subsurface.” Finally, the filenames themselves identify the incident ion species, with atomic number Z and mass number A for the most abundant isotopes of ions from Z = 01 to 28 (H to Ni), plus ^3He ; the ion in the example filename above is ^{58}Ni . Thus a single subdirectory contains the kernel files for all primary ion species that address the production of a single albedo species (or category, for “heavy_helium,” “z_gt_2,” or “misc”) with a single target geometry (upper layer composition and slab thickness) and tabulation altitude.

3.1.2 Energy/Angle Examples

In each of the subdirectories described in Section 3.1.1, alongside the “ion_ZZ_AA.json” files, are six files that can be used to exercise the model and check that it has been imported into users’ code correctly. There are two JSON files containing spectra from the Badhwar-O’Neill 2020 cosmic-ray model (Slaba & Whitman, 2020) for periods corresponding to the least (solar minimum) and greatest (solar maximum) solar modulation identified in LRO/CRaTER observations over the past solar activity cycle (Looper et al., 2020); the two files, “solmin_gcr.json” and “solmax_gcr.json,” are the same in each of the subdirectories enumerated in Section 3.1.1. Convolution of each of the primary-ion spectra in these files (^3He is not included in the Badhwar-O’Neill 2020 model output) with the ion’s respective kernel as in Equation (4) and summing over all primary ions gives the total energy/angle distribution for the secondary-particle species covered by the subdirectory. These distributions are stored in JSON files and plotted as PNG images with names incorporating the solar cycle designation and the subdirectory name; e.g., the example subdirectory given in Section 3.1.1 will contain “solmax_electrons_20_km_altitude.json” and “solmin_electrons_20_km_altitude.json,” and also *.png files with corresponding names.

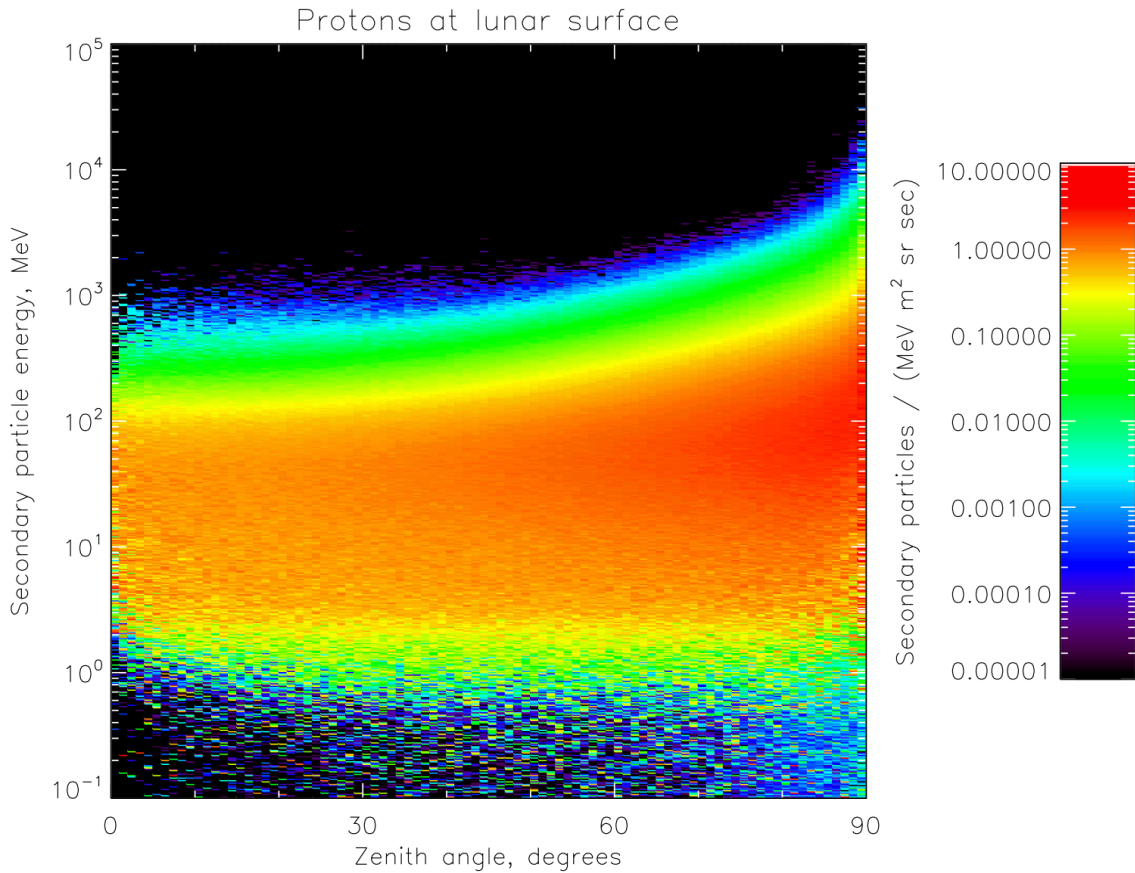


Figure 3: Plot of example output stored in one subdirectory. This is the energy/angle distribution of the albedo proton flux modeled at the surface for solar-minimum cosmic-ray spectra striking the dry FAN target.

Figure 3 reproduces the plot in

`dry_10cm_protons/protons_surface/solmin_protons_surface.png`

which is representative of the result images stored in the subdirectories. This is the energy/angle distribution of albedo protons produced by the solar-minimum cosmic-ray spectra incident on the dry FAN target and tabulated at the lunar surface. Earlier versions of this plot have been shown as part of previous work by the LRO/CRaTER team (e.g., Schwadron et al., 2016, 2018), and refinement of that work is why this model was developed.

3.1.3 Energy/Angle/Depth Kernels

The JSON files storing the energy/angle/depth kernels $S_j(E_i, E_j, D, \theta_j)$, as defined in Equation (5) for albedo protons and neutrons, are collected into a separate set of zipfiles for base directories ending in “_origins” and with the same target-geometry prefixes as the energy/angle files (“dry_10cm_origins,” etc.). In each of these are three subdirectories named “neutrons_inelastic,” “protons_inelastic,” and “protons_elastic,” which collect model results for

the two source-process possibilities for protons (elastic and inelastic) and the one for neutrons (inelastic), as discussed in Section 2.2. As in the energy/angle directories, the energy/angle/depth kernels for individual incident ion species are stored in JSON files with names of the form ion_ZZ_AA.json. Thus, for example, one full filepath would be

```
dry_10cm_origins/neutrons_inelastic/ion_01_01.json
```

3.1.4 Backscattered Proton Kernels

Also, as noted at the end of Section 2.2, primary protons that scatter back out of the surface all have zero depth of origin, so their full energy/angle kernels (with 90 angular bins rather than 3) are stored in the same format as the energy/angle files for albedo protons, and in the same base directory but in their own subdirectory named “protons_primary.” Thus, for example, the kernel for the portion of the results shown in Figure 3 that is due to backscattered protons will be stored as

```
dry_10cm_protons/protons_primary/ion_01_01.json
```

3.1.5 Energy/Angle/Depth Examples

Similarly to the content of the energy/angle portion of the model discussed in Section 3.1.2, each of the subdirectories in the “_origins” base directories also contains files that users can reproduce to check their importing and use of the model files. The same two JSON files of cosmic-ray spectra from the Badhwar-O’Neill 2020 model are present, along with JSON files and PNG images of the energy/angle/depth distributions of albedo particles that result from convolution of the response kernels with these cosmic-ray spectra. As described in Section 2.2, the angular information for the albedo protons or neutrons is collected into three broad bins of zenith angle; thus the convolution products presented in the PNG images are energy/depth distributions for each of the three angle bins separately. The file naming convention is similar to that outlined in Section 3.1.2, with “solmin_” or “solmax_” followed by the subdirectory name for the JSON files, and adding “_00_30,” “_30_60,” or “_60_90” for the angular bin in each PNG file.

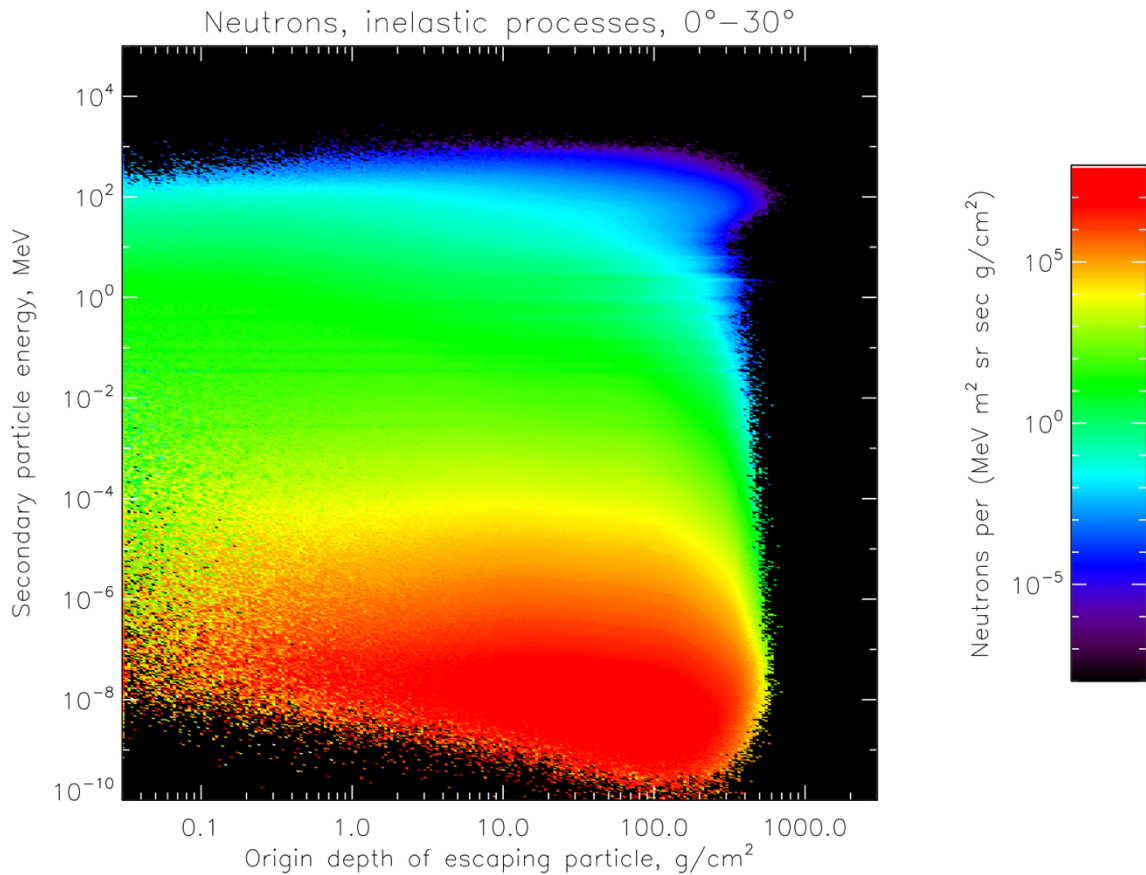


Figure 4: Plot of example output stored in one energy/angle/depth subdirectory. This is the energy/depth distribution of the albedo neutron flux modeled at the surface for solar-minimum cosmic-ray spectra striking the dry FAN target, averaged over zenith angles from 0° to 30°.

Figure 4 reproduces the plot in

`dry_10cm_origins/neutrons_inelastic/solmin_neutrons_inelastic_00_30.png`

As discussed in Section 2.2, the dimensions of the modeled observable quantity here are those of the directional differential albedo particle flux, further differentiated by depth in units of column mass density (g/cm^2). Given the 3.0 g/cc density of the modeled FAN target, it can be seen that the neutrons escaping from the surface come from depths down to only about 2 meters, which indicates that the 20 m thickness of the modeled target slab is ample to contain the nuclear (and electromagnetic) showers that result from the impact even of high-energy cosmic rays.

3.1.6 Backscattered Proton Examples

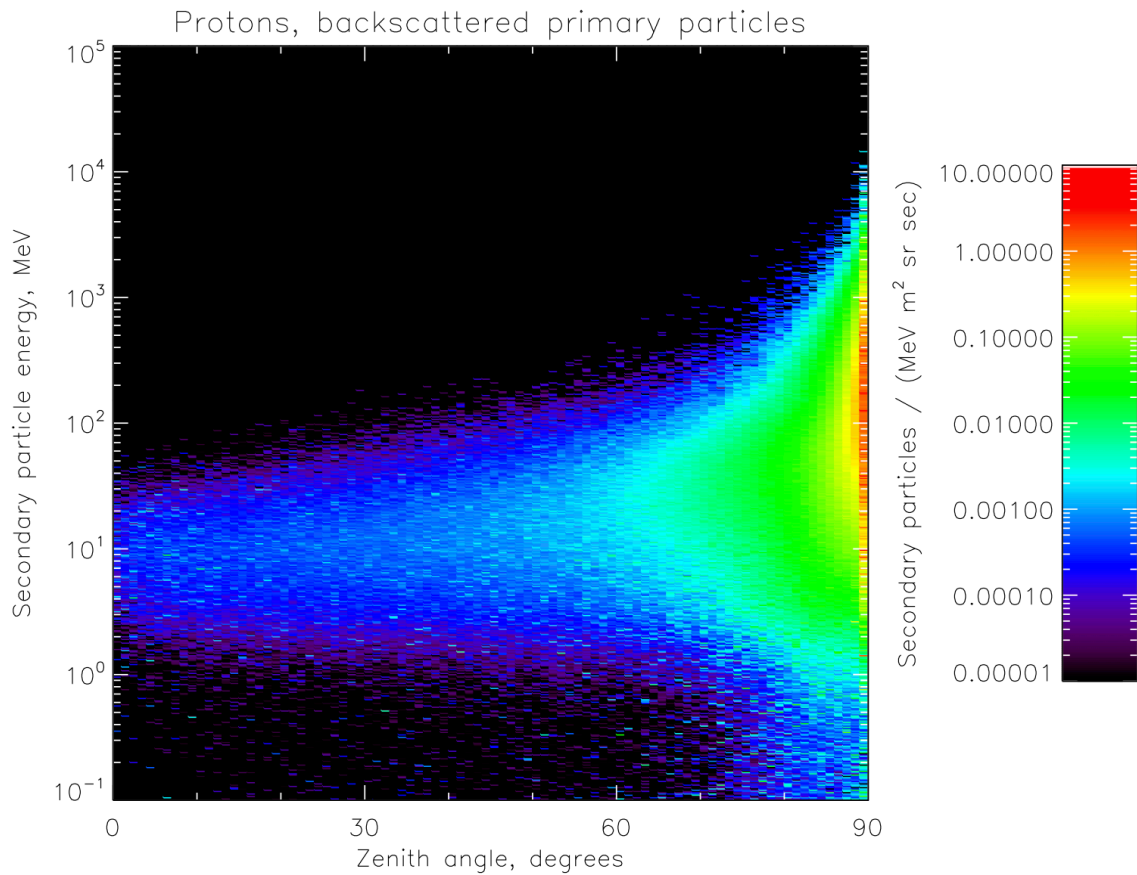


Figure 5: Plot of example output for one set of backscattered primary protons. This is the energy/angle distribution of the albedo proton flux due to backscattering of primary cosmic-ray protons modeled at the surface for the solar-minimum cosmic-ray spectrum striking the dry FAN target. These particles are a subset of those plotted in Figure 3; colorscale is the same.

The set of example files – cosmic ray spectra and convolved energy/angle distributions – is also provided for the backscattered primary cosmic-ray protons, again with similar naming conventions. The plot in

`dry_10cm_protons/protons_primary/solmin_protons_primary.png`

is reproduced in Figure 5; the axes and colorscale are the same as in Figure 3 for the full energy/angle distribution of albedo protons from all sources (all primary ions, all processes) for the same cosmic-ray primary spectra striking the dry FAN target.

3.2 Contents of Model Files

The JSON format is easily human- and machine-readable. For example, the files were assembled from the Geant4 simulation results using IDL, and in this language, importing the contents of a JSON file into a data structure is as simple as

```

json = ''
openr,1,'filename.json'
readf,1,json
close,1
data = json_parse(json,/toarray,/tostruct)

```

In constructing these files, we have included metadata in each one. The tables below summarize the metadata and data contents of each kind of JSON file discussed in Section 3.1, which would be encapsulated in the structure “data” in the IDL code fragment above. Note that numbers, denoted under “Variable Type” by dimensions or sets of dimensions in square braces, are of double-precision floating point numbers in the JSON files, or in one case (labeled “Integer[28]”) long integers. However, whether that precision is preserved upon import will depend on the user code employed for analysis.

Table 1 – Energy/Angle Kernel Files

Variable Name	Variable Type	Description
LUNAR_TARGET	String	One of the 16 target layer geometries
OBSERVER_ELEVATION	String	Surface, 20 km altitude, or subsurface
PRIMARY_ION_SPECIES	String	Values of Z and A for incident ion
SECONDARY_PARTICLE_SPECIES	String	One of the 16 albedo species or groups
GEANT4_ENVIRONMENT	String	Geant4 version and physics list used
GLACE_VERSION	String	Version of GLACE model
PRIMARY_ENERGY_UNITS	String	Units of PRIMARY_ENERGY_BINS
SECONDARY_ENERGY_UNITS	String	Units of SECONDARY_ENERGY_BINS
SECONDARY_ZENITH_ANGLE_UNITS	String	Units of SECONDARY_ZENITH_ANGLE_BINS
RESPONSE_UNITS	String	Units of RESPONSE, RESPONSE_SIGMA
PRIMARY_ENERGY_BINS	[201]	Edges of 200 E_i bins
SECONDARY_ENERGY_BINS	[601]	Edges of 600 E_j bins
SECONDARY_ZENITH_ANGLE_BINS	[91]	Edges of 90 θ_j bins
RESPONSE	[200,600,90]	Simulated values of $R_j(E_i, E_j, \theta_j)$
RESPONSE_SIGMA	[200,600,90]	Standard deviation of $R_j(E_i, E_j, \theta_j)$

Table 2 – Energy/Angle/Depth Kernel Files

Variable Name	Variable Type	Description
LUNAR_TARGET	String	One of the 16 target layer geometries
OBSERVER_ELEVATION	String	“At lunar surface” only
PRIMARY_ION_SPECIES	String	Values of Z and A for incident ion
SECONDARY_ORIGIN_PROCESS	String	Elastic or inelastic processes
SECONDARY_PARTICLE_SPECIES	String	Neutrons or protons
GEANT4_ENVIRONMENT	String	Geant4 version and physics list used
GLACE_VERSION	String	Version of GLACE model
PRIMARY_ENERGY_UNITS	String	Units of PRIMARY_ENERGY_BINS
SECONDARY_ENERGY_UNITS	String	Units of SECONDARY_ENERGY_BINS
SECONDARY_ORIGIN_DEPTH_UNITS	String	Units of SECONDARY_ORIGIN_DEPTH_BINS
SECONDARY_ZENITH_ANGLE_UNITS	String	Units of SECONDARY_ZENITH_ANGLE_BINS
RESPONSE_UNITS	String	Units of RESPONSE, RESPONSE_SIGMA
PRIMARY_ENERGY_BINS	[201]	Edges of 200 E_i bins
SECONDARY_ENERGY_BINS	[601]	Edges of 600 E_j bins
SECONDARY_ORIGIN_DEPTH_BINS	[251]	Edges of 250 D_j bins
SECONDARY_ZENITH_ANGLE_BINS	[4]	Edges of 3 θ_j bins
RESPONSE	[200,600,250,3]	Simulated values of $S_j(E_i, E_j, D_j, \theta_j)$
RESPONSE_SIGMA	[200,600,250,3]	Standard deviation of $S_j(E_i, E_j, D_j, \theta_j)$

Table 3 – Energy/Angle Kernel Files for Backscattered Protons

Variable Name	Variable Type	Description
LUNAR_TARGET	String	One of the 16 target layer geometries
OBSERVER_ELEVATION	String	“At lunar surface” only
PRIMARY_ION_SPECIES	String	“Z = 1, A = 1” only
SECONDARY_ORIGIN_PROCESS	String	“Backscattered primary particle”
SECONDARY_PARTICLE_SPECIES	String	“Protons” only
GEANT4_ENVIRONMENT	String	Geant4 version and physics list used
GLACE_VERSION	String	Version of GLACE model
PRIMARY_ENERGY_UNITS	String	Units of PRIMARY_ENERGY_BINS
SECONDARY_ENERGY_UNITS	String	Units of SECONDARY_ENERGY_BINS
SECONDARY_ZENITH_ANGLE_UNITS	String	Units of SECONDARY_ZENITH_ANGLE_BINS
RESPONSE_UNITS	String	Units of RESPONSE, RESPONSE_SIGMA
PRIMARY_ENERGY_BINS	[201]	Edges of 200 E_i bins
SECONDARY_ENERGY_BINS	[601]	Edges of 600 E_j bins
SECONDARY_ZENITH_ANGLE_BINS	[91]	Edges of 90 θ_j bins
RESPONSE	[200,600,90]	Simulated values of $R_j(E_i, E_j, \theta_j)$
RESPONSE_SIGMA	[200,600,90]	Standard deviation of $R_j(E_i, E_j, \theta_j)$

Table 4 – Badhwar-O’Neill 2020 (BON2020) Galactic Cosmic Ray Spectra Files

Variable Name	Variable Type	Description
BON_CODE_VERSION	String	Badhwar-O’Neill 2020 model version
RUN_DATES	String	Start and end dates for BON2020 run
PHI_UNITS	String	Units of RUN_PHI
ENERGY_UNITS	String	Units of GCR_ENERGIES
FLUX_UNITS	String	Units of GCR_FLUXES
RUN_PHI	[1]	Modulation potential for BON2020 run
GCR_Z	Integer[28]	Atomic numbers of 28 cosmic-ray primary ion species
GCR_ENERGIES	[100]	Energies E_i at which GCR_FLUXES are calculated
GCR_FLUXES	[28,100]	Fluxes of 28 primary-ion species at 100 energies E_i

Table 5 – Energy/Angle Example Files

Variable Name	Variable Type	Description
BON_CODE_VERSION	String	Badhwar-O’Neill 2020 model version
RUN_DATES	String	Start and end dates for BON2020 run
LUNAR_TARGET	String	One of the 16 target layer geometries
OBSERVER_ELEVATION	String	Surface, 20 km altitude, or subsurface
SECONDARY_PARTICLE_SPECIES	String	One of the 16 albedo species or groups
GEANT4_ENVIRONMENT	String	Geant4 version and physics list used
GLACE_VERSION	String	Version of GLACE model
PHI_UNITS	String	Units of RUN_PHI
SECONDARY_ENERGY_UNITS	String	Units of SECONDARY_ENERGY_BINS
SECONDARY_ZENITH_ANGLE_UNITS	String	Units of SECONDARY_ZENITH_ANGLE_BINS
SECONDARY_FLUX_UNITS	String	Units of SECONDARY_FLUX
RUN_PHI	[1]	Modulation potential for BON2020 run
SECONDARY_ENERGY_BINS	[601]	Edges of 600 E_j bins
SECONDARY_ZENITH_ANGLE_BINS	[91]	Edges of 90 θ_j bins
SECONDARY_FLUX	[600,90]	Convolved values of $J_j(E_j, \theta_j)$

Table 6 – Energy/Angle/Depth Example Files

Variable Name	Variable Type	Description
BON_CODE_VERSION	String	Badhwar-O’Neill 2020 model version
RUN_DATES	String	Start and end dates for BON2020 run
LUNAR_TARGET	String	One of the 16 target layer geometries
OBSERVER_ELEVATION	String	“At lunar surface” only
SECONDARY_ORIGIN_PROCESS	String	Elastic or inelastic processes
SECONDARY_PARTICLE_SPECIES	String	Neutrons or protons
GEANT4_ENVIRONMENT	String	Geant4 version and physics list used
GLACE_VERSION	String	Version of GLACE model
PHI_UNITS	String	Units of RUN_PHI
SECONDARY_ENERGY_UNITS	String	Units of SECONDARY_ENERGY_BINS
SECONDARY_ORIGIN_DEPTH_UNITS	String	Units of SECONDARY_ORIGIN_DEPTH_BINS
SECONDARY_ZENITH_ANGLE_UNITS	String	Units of SECONDARY_ZENITH_ANGLE_BINS
SECONDARY_FLUX_UNITS	String	Units of SECONDARY_FLUX
RUN_PHI	[1]	Modulation potential for BON2020 run
SECONDARY_ENERGY_BINS	[601]	Edges of 600 E_j bins
SECONDARY_ORIGIN_DEPTH_BINS	[251]	Edges of 250 D_j bins
SECONDARY_ZENITH_ANGLE_BINS	[4]	Edges of 3 θ_j bins
SECONDARY_FLUX	[600,250,3]	Convolved values of $Q_j(E_j, D_j, \theta_j)$

Table 7 – Energy/Angle Example Files for Backscattered Protons

Variable Name	Variable Type	Description
BON_CODE_VERSION	String	Badhwar-O’Neill 2020 model version
RUN_DATES	String	Start and end dates for BON2020 run
LUNAR_TARGET	String	One of the 16 target layer geometries
OBSERVER_ELEVATION	String	“At lunar surface” only
SECONDARY_ORIGIN_PROCESS	String	“Backscattered primary particle”
SECONDARY_PARTICLE_SPECIES	String	“Protons” only
GEANT4_ENVIRONMENT	String	Geant4 version and physics list used
GLACE_VERSION	String	Version of GLACE model
PHI_UNITS	String	Units of RUN_PHI
SECONDARY_ENERGY_UNITS	String	Units of SECONDARY_ENERGY_BINS
SECONDARY_ZENITH_ANGLE_UNITS	String	Units of SECONDARY_ZENITH_ANGLE_BINS
SECONDARY_FLUX_UNITS	String	Units of SECONDARY_FLUX
RUN_PHI	[1]	Modulation potential for BON2020 run
SECONDARY_ENERGY_BINS	[601]	Edges of 600 E_j bins
SECONDARY_ZENITH_ANGLE_BINS	[91]	Edges of 90 θ_j bins
SECONDARY_FLUX	[600,90]	Convolved values of $J_j(E_j, \theta_j)$

4. Acknowledgements

This work was supported by NASA under contract NNG11PA03C.

5. References

Agostinelli, J., et al., “Recent Developments in Geant4,” *Nucl. Inst. And Meth. In Phys. Res. A*, **835**, pp. 186-225, DOI: 10.1016/j.nima.2016.06.125 (2016)

Looper, M. D., J. E. Mazur, J. B. Blake, H. E. Spence, N. A. Schwadron, J. K. Wilson, A. P. Jordan, C. Zeitlin, A. W. Case, J. C. Kasper, L. W. Townsend, and T. J. Stubbs, “Long-Term Observations of Galactic Cosmic Ray LET Spectra in Lunar Orbit by LRO/CRaTER,” *Space Weather* **18** (12), e2020SW002543, DOI: 10.1029/2020SW002543 (2020)

Schwadron, N. A., J. K. Wilson, M. D. Looper, A. P. Jordan, H. E. Spence, J. B. Blake, A. W. Case, Y. Iwata, J. C. Kasper, W. M. Farrell, D. J. Lawrence, G. Livadiotis, J. Mazur, N. Petro, C. Pieters, M. S. Robinson, S. Smith, L. W. Townsend, and C. Zeitlin, “Signatures of Volatiles in the Lunar Proton Albedo,” *Icarus* **273**, pp. 25-35, DOI: 10.1016/j.icarus/2015.12.003 (2016)

Schwadron, N. A., J. K. Wilson, A. P. Jordan, M. D. Looper, C. Zeitlin, L. W. Townsend, H. E. Spence, J. Legere, P. Bloser, W. M. Farrell, D. Hurley, N. Petro, T. J. Stubbs, and C. Pieters, "Using Proton Radiation from the Moon to Search for Diurnal Variation of Regolith Hydrogenation," *Planetary and Space Sci.* **162**, pp. 113-132, DOI: 10.1016/j.pss/2017.09.012 (2018)

Slaba, T. C., and K. Whitman, "The Badhwar-O'Neill 2020 GCR Model," *Space Weather* **18** (6), e2020SW002456, DOI: 10.1029/2020SW002456 (2020)

Appendix

The following tables show the compressed and uncompressed sizes and the contents of each of the 96 base directories and their zipfiles that compose the GLACE model. For the first two tables, the rows are the sixteen target geometries, and columns are the six subsets into which the kernel files for each are divided. The third table gives the number of each kind of constituent file or subdirectory in a base directory with the given suffix, which will be the same for all sixteen target geometries. Tables A1 and A2 give the sizes in gigabytes, defined as 10^9 bytes; for sizes in "binary gigabytes," or 2^{30} bytes, divide these numbers by 1.074.

Table A1 – Sizes of Uncompressed Base Directories

	_electrons	_gammas	_neutrons	_origins	_other	_protons
dry_10cm_	6.70 GB	9.46 GB	16.96 GB	69.10 GB	61.06 GB	5.71 GB
h1pct_1mm_	6.67 GB	9.49 GB	16.41 GB	69.13 GB	61.03 GB	5.72 GB
h1pct_1cm_	6.68 GB	9.53 GB	16.42 GB	68.75 GB	61.02 GB	5.72 GB
h1pct_10cm_	6.66 GB	9.50 GB	13.33 GB	65.60 GB	61.03 GB	5.71 GB
h1pct_1m_	6.64 GB	9.37 GB	11.40 GB	65.35 GB	61.03 GB	5.71 GB
h1pct_10m_	6.64 GB	9.37 GB	9.84 GB	65.35 GB	60.94 GB	5.70 GB
h10pct_1mm_	6.69 GB	9.47 GB	16.34 GB	69.11 GB	61.06 GB	5.71 GB
h10pct_1cm_	6.69 GB	9.47 GB	16.55 GB	69.17 GB	61.06 GB	5.71 GB
h10pct_10cm_	6.72 GB	9.53 GB	16.43 GB	68.48 GB	61.06 GB	5.71 GB
h10pct_1m_	6.70 GB	9.49 GB	13.91 GB	67.32 GB	61.06 GB	5.71 GB
h10pct_10m_	6.70 GB	9.49 GB	11.72 GB	67.31 GB	61.06 GB	5.71 GB
h2o9pct_1mm_	6.69 GB	9.46 GB	16.34 GB	69.11 GB	61.06 GB	5.71 GB
h2o9pct_1cm_	6.69 GB	9.46 GB	16.56 GB	69.16 GB	61.05 GB	5.71 GB
h2o9pct_10cm_	6.72 GB	9.53 GB	16.40 GB	68.43 GB	61.06 GB	5.71 GB
h2o9pct_1m_	6.70 GB	9.50 GB	13.88 GB	67.28 GB	61.06 GB	5.71 GB
h2o9pct_10m_	6.70 GB	9.50 GB	11.69 GB	67.29 GB	61.06 GB	5.71 GB

Table A2 – Sizes of Compressed Base-Directory Zipfiles

	_electrons	_gammas	_neutrons	_origins	_other	_protons
dry_10cm_	1105 MB	2793 MB	6049 MB	4169 MB	624 MB	383 MB
h1pct_1mm_	1090 MB	2812 MB	5707 MB	4200 MB	606 MB	388 MB
h1pct_1cm_	1094 MB	2837 MB	5737 MB	4025 MB	598 MB	389 MB
h1pct_10cm_	1086 MB	2816 MB	3756 MB	1987 MB	598 MB	382 MB
h1pct_1m_	1070 MB	2738 MB	2565 MB	1822 MB	600 MB	379 MB
h1pct_10m_	1070 MB	2738 MB	1507 MB	1822 MB	599 MB	379 MB
h10pct_1mm_	1104 MB	2796 MB	5663 MB	4175 MB	622 MB	384 MB
h10pct_1cm_	1104 MB	2797 MB	5798 MB	4225 MB	622 MB	384 MB
h10pct_10cm_	1121 MB	2835 MB	5741 MB	3840 MB	625 MB	384 MB
h10pct_1m_	1109 MB	2814 MB	4177 MB	3072 MB	624 MB	384 MB
h10pct_10m_	1109 MB	2813 MB	2726 MB	3071 MB	623 MB	384 MB
h2o9pct_1mm_	1102 MB	2795 MB	5663 MB	4173 MB	621 MB	382 MB
h2o9pct_1cm_	1102 MB	2796 MB	5801 MB	4220 MB	619 MB	382 MB
h2o9pct_10cm_	1119 MB	2834 MB	5723 MB	3812 MB	624 MB	382 MB
h2o9pct_1m_	1109 MB	2814 MB	4159 MB	3053 MB	624 MB	382 MB
h2o9pct_10m_	1109 MB	2814 MB	2710 MB	3054 MB	624 MB	382 MB

Table A3 – Number of Subdirectories and Files in Each Base Directory

	_electrons	_gammas	_neutrons	_origins	_other	_protons
Subdirectories	2	2	3	3	24	3
JSON kernel files	58	58	87	87	696	59
JSON example files	8	8	12	12	96	12
PNG example files	4	4	6	18	48	6